PAPER • OPEN ACCESS

Manipulating the topological structure of ultrarelativistic electron beams using Laguerre–Gaussian laser pulse

To cite this article: L B Ju *et al* 2018 *New J. Phys.* **20** 063004

New Journal of Physics
The open access journal at the forefront of physics

Deutsche Physikalische Gesellschaft DPG
IOP Institute of Physics

Published in partnership with: Deutsche Physikalische Gesellschaft and the Institute of Physics

OPEN ACCESS

RECEIVED
8 January 2018

REVISED
23 April 2018

ACCEPTED FOR PUBLICATION
21 May 2018

PUBLISHED
5 June 2018

PAPER

Manipulating the topological structure of ultrarelativistic electron beams using Laguerre–Gaussian laser pulse

L B Ju[1,2], C T Zhou[1,2,4,5,6], K Jiang[3,4], T W Huang[1,2,6], H Zhang[1,4], T X Cai[1], J M Cao[1], B Qiao[1,5] and S C Ruan[1,2]

[1] Center for Advanced Material Diagnostic Technology, Shenzhen Technology University, Shenzhen 518118, People's Republic of China
[2] College of Optoelectronic Engineering, Shenzhen University, Shenzhen 518060, People's Republic of China
[3] Graduate School, China Academy of Engineering Physics, Beijing 100088, People's Republic of China
[4] Institute of Applied Physics and Computational Mathematics, Beijing 100094, People's Republic of China
[5] HEDPS, Center for Applied Physics and Technology and School of Physics, Peking University, Beijing 100871, People's Republic of China
[6] Author to whom any correspondence should be addressed

E-mail: zcangtao@sztu.edu.cn **and** taiwu.huang@szu.edu.cn

Keywords: laser–plasma interaction, Laguerre–Gaussian laser pulse, electron acceleration mechanism, vortex electron beams

Abstract

A method of using intense Laguerre–Gaussian (LG) laser pulse is proposed to generate ultrarelativistic (multi-GeV) electron beams with controllable helical structures based on a hybrid electron acceleration regime in underdense plasmas, where both the longitudinal charge-separation electric field and transverse laser electric field play the role of accelerating the electrons. By directly interacting with the LG laser pulse, the topological structure of the accelerated electron beam is manipulated and it is spatially separated into multi-slice helical bunches. These results are clearly demonstrated by our three-dimensional particle-in-cell simulations and explained by a theoretical model based on electron phase-space dynamics. This novel regime offers a new degree of freedom for manipulating ultrashort and ultrarelativistic electrons, and it provides an efficient way for generating high-energy high-angular-momentum helical electron beams, which may find applications in wide-ranging areas.

1. Introduction

Vortex light beams, which carry a finite orbital angular momentum (OAM), are characterized by an angular-dependant phase $\Phi = l\phi$ with helical wavefront and strictly zero intensity on the propagation axis [1], where l is the topological charge that indicates the OAM carried by each photon and ϕ is the azimuthal angle. Such vortex light beams are described by Laguerre–Gaussian (LG) modes, which can be implemented by several techniques such as mode conversion from Hermite–Gaussian to LG, using spiral phase plates, computer holograms, etc [2–5]. They are widely used in applications such as optical microscopy, micromanipulation, quantum information, astronomy, etc [6–10]. Recently, vortex laser pulses with relativistic intensities are also achieved based on the techniques of plasma holograms [11], Raman amplification [12], and the light fan [13], which have stimulated much research interest in intense laser–matter interactions and extended the study of OAM into a relativistic regime [14–18].

In addition to the vortex laser beams, particle beams such as electrons [19–21], neutrons [22], and x/gamma-ray photons [23–28], can also carry OAM. In particular, electron vortex beams carrying OAM have extensive applications ranging from condensed-matter spectroscopy and new electron microscopes, to particle physics [19–24, 29, 30]. Electron vortex beams can be generated through the spiral phase plate and computer-generated holograms in a transmission electron microscope [19–21]. However, so far the achieved electron vortex beams are limited to a nonrelativistic energy range. Relativistic electron vortex beams are still unavailable based on the existing techniques. Recently, laser-based plasma accelerators have attracted much research attention, which can produce monoenergetic electron beams with energies up to several GeV in the so-called laser wake field acceleration (LWFA) regime [31–39]. In addition, when the intense laser pulse interacts with the plasma, its angular momentum can be transferred into electrons when the conservativeness of photon number is

broken during nonlinear laser–plasma interactions [40–42]. Thus, it would be possible to manipulate the topological structure of relativistic electron beams and generate high-energy high-OAM electron beams based on laser–plasma interactions.

In this paper, we demonstrate for the first time that ultrarelativistic screw-like electrons beams with high-OAM can be produced by exploiting a hybrid electron acceleration regime driven by an intense LG laser pulse in undersense plasmas. In this regime, electrons are accelerated by the longitudinal charge-separation electric field and also the transverse laser electric field. Meanwhile, the LG laser pulse effectively transfers its angular momentum to the accelerated electron beam and manipulates the topological structure of the electron beam. Our three-dimensional (3D) particle-in-cell (PIC) simulations show that in this regime, the accelerated electron beam is spatially separated and consists of multi-slice helical bunches. A theoretical model based on the electron phase-space dynamics is also proposed to explain the emergence of multi-slice helical electron bunches. It is clarified that the topological charge of the LG laser pulse determines the number of fixed points in the system, which in turn determines the number of electron bunches that are accelerated in different phases of the laser electric field. In this way, the topological structure of the electron beam can be well controlled by adjusting the laser's topological charge.

2. Simulation and results

In order to investigate the interaction process of intense LG laser pulse with underdense plasmas, 3D PIC simulations were performed using EPOCH code [43]. A LG laser pulse with central wavelength $\lambda = 800$ nm and laser period $T_L = \lambda/c$ is normally incident from the left boundary ($x = 0$), where c is the speed of light in vacuum and x is the laser propagation axis. The transverse profile of a LG laser with zero radial index at $x = 0$ is

$$\vec{a}(r) = a_0(\vec{e}_y + \sigma\vec{e}_z)\left(\frac{\sqrt{2}\,r}{r_0}\right)^{|l|}\exp\left(-\frac{r^2}{r_0^2}\right)\exp(-\mathrm{i}l\theta), \tag{1}$$

where a_0 is the normalized amplitude of laser electric field, $r = \sqrt{y^2 + z^2}$, r_0 is the laser beam radius, θ is the azimuthal angle in transverse space, l is the topological charge of LG laser pulse, $\vec{e}_y$, $\vec{e}_z$ are the unit vectors in y and z direction, and σ represents the laser polarization state. σ is equal to 1 or -1 for right-hand and left-hand circular polarization, respectively. For linear polarization, σ is equal to 0. Here a right-hand circularly polarized (CP) LG laser is considered. In the simulations, LG laser pulses with different topological charges ($l = 0, 1, 2$) are employed. In particular, for $l = 0$, the LG laser pulse is reduced into the normal Gaussian laser pulse. In these simulations, the value of a_0 is set as 70, the initial laser beam radius is set as $r_0 = 7\lambda$, and the duration (τ) of the laser pulse is set as $20T_L$. The plasma is located in the region of $5\lambda < x < 100\lambda$ with a uniform density of $n_e = 2.4 \times 10^{20}\,\mathrm{cm}^{-3}$. The initial electron temperature is assumed to be 1 keV and ion temperature is 30 eV. The simulation box is $100\lambda(x) \times 25\lambda(y) \times 25\lambda(z)$ with a grid of $1000 \times 250 \times 250$ and four particles per cell. In the current setup, the laser pulse length ($c\tau$) is comparable with the size of the plasma bubble ($2\lambda\sqrt{a_l n_c/n_e}/\pi$) created by the ultraintense laser pulse, were $n_c \approx 1.74 \times 10^{21}\,\mathrm{cm}^{-3}$ refers to the critical plasma density and $a_l = a_0 l^l \exp(-l/2)$ is the amplitude of the LG laser pulse. In this case, the self-injected electrons can interact with the laser field directly when they are accelerated by the longitudinal charge-separation electric field [44, 45].

When the intense LG laser pulse propagates into the underdense plasma, its ponderomotive force expels the electrons from the laser region. For the LG laser pulse, because there is no component of laser electric field on the central axis, as shown in figure 1(a), the electrons are expelled both outward and inward around the LG laser pulse in transverse space. As a result, a donut-like plasma bubble with a compressed plasma pillar along the central axis is formed, as shown in figure 1(d). In the plasma bubble, quasistatic electromagnetic fields are also generated, as shown in figures 1(b) and (c). The transverse focusing field, which consists of the transverse charge-separation electric field E_{Sr} and azimuthal magnetic field $B_{S\theta}$, can be expressed as $(E_{Sr} - cB_{S\theta})$ and is shown in figure 1(b). Under these intense fields, the self-injected electrons are trapped and confined in the donut-like plasma bubble, and experience betatron oscillations, as shown in figure 1(d). Meanwhile, these electrons are accelerated longitudinally at the rear of the donut bubble by the negative longitudinal charge-separation electric field E_{Sx}, as shown in figure 1(c). For a LG laser pulse with $l = 2$, $a_l = a_0 l^l \exp(-l/2) \approx 103$, the bubble size can be estimated as $2\lambda\sqrt{a_l n_c/n_e}/\pi \approx 17.4\lambda$, which is in good agreement with the simulation results shown in figure 1(d). For these parameters, the bubble size is comparable with the laser pulse length (20λ), which indicates a significant overlap between the trapped electrons and the transverse laser field, as can be seen in figures 1(a) and (d). In this case, the electrons can be directly accelerated by the transverse laser field, once the betatron oscillation frequency of the electrons is close to the Doppler-shifted laser frequency [46]. In this process, the trapped electrons are microbunched with the laser wavelength, as shown figure 1(d), which is indicative of direct laser acceleration (DLA) [47]. By directly interacting with the laser field, the electrons gain energy and angular

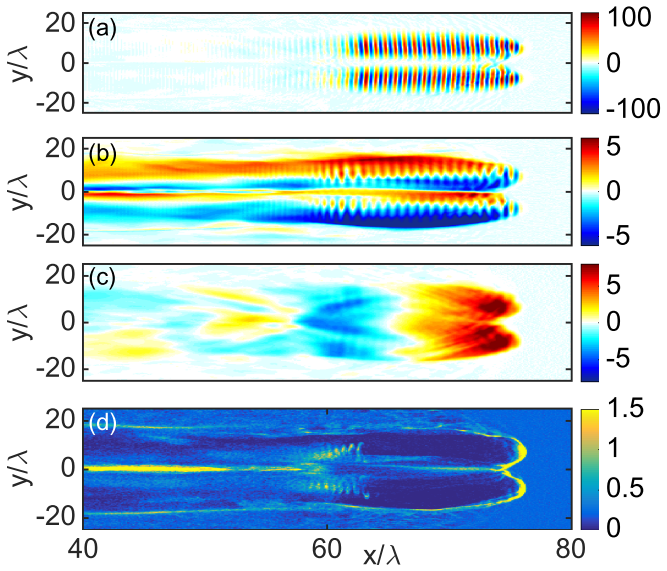

Figure 1. (a) The transverse distribution of the normalized laser electric field in units of $m_e\omega\, c/e$ at $20T_L$ for $l = 2$; (b) the corresponding quasistatic focusing fields $E_r - cB_\theta$ in units of $m_e\omega\, c/e$; (c) the longitudinal charge-separation field E_{Sx} in units of $m_e\omega\, c/e$; (d) the electron density normalized by n_c.

momentum (both spin and orbit angular momentum) simultaneously from the LG laser pulse [17], as a result, they are manipulated by the laser pulse and distributed as helical structures, as indicated in figure 1(d).

The corresponding 3D distribution of the high-energy electrons in the plasma bubble is shown in figure 2 for LG laser pulses with different topological charges l. It is clearly demonstrated that the high-energy electrons are helically distributed in space due to the interaction with the LG laser pulse, which efficiently transfers its angular momentum into these electrons. In particular, the electron beam displays as multi-slice helical bunches and the number of the electron bunches is determined by the topological charge of the LG laser pulse. For example, there is only one slice for $l = 0$, as shown in figure 2(a).When $l = 0$, the LG laser pulse is reduced into a CP Gaussian laser pulse. In this case, the resonant electrons in the plasma bubble are locked in the acceleration phase of CP laser field and they experience circular motions collectively together with the rotating CP laser field. As a result, the energy density of the accelerated electron beam exhibits an annular distribution, as shown in figure 2(a), which also agrees well with previous simulation results using CP Gaussian laser pulse [17, 45]. However, for $l \neq 0$, the results are quite different from the case with $l = 0$. For $l = 1$, there are two helical electron bunches intertwined each other, as shown in figure 2(b), and the number of the intertwined electrons bunches becomes 3 for $l = 2$, as shown in figure 2(c).

The energy spectra of the helical electron beams are plotted in figure 3(a), which shows that the accelerated electrons display as peaked energy spectra for different cases. The electron energy at the peaks is about 1 GeV and the maximum energy can reach up to 2.0 GeV. The corresponding OAM of the accelerated electrons is calculated as $L = yp_z - zp_y$, where p_y, p_z are the linear momentum of particles in y and z direction, respectively. Figure 3(b) shows that the OAM of electrons increases linearly with time [17]. It is obvious that electrons cannot gain OAM when they are only accelerated longitudinally by the charge-separation field E_{Sx} at the rear of the plasma bubble. Once the electrons catch up with the tail of LG laser pulse, they get OAM directly from the laser. It is shown from figure 3(b) that the OAM of the high-energy electrons (normalized by $\lambda\, m_e c$) can reach up to -1.75×10^{14}, -3.5×10^{14}, and -4.5×10^{14} for $l = 0, 1, 2$, respectively. The total angular momentum of the LG laser pulse can be calculated as $L_x \approx -(l + \sigma)\frac{I_0 \pi r_0^2 \tau}{2\omega_0}$, where σ is determined by the laser polarization state, $I_0 = m_e c^3 n_c a_l^3$ is the peak laser intensity, and ω_0 refers to the central laser frequency. For the right-hand CP laser pulse, $\sigma = 1$. When $l = 0$, the OAM of the LG laser is zero, but the CP laser pulse itself still carries spin angular momentum. In this case, the accelerated electrons can still gain angular momentum from the laser pulse [17]. In the simulations, the conversion rate of the angular momentum from laser to electrons is about 30% for these three cases, which is comparable with the energy conversion rate. This indicates that the OAM of the electron beam is proportional to the value of $l + 1$. In order to clarify the acceleration mechanism of the high-energy electrons, particle tracing methods were carried out here. The energy gain of electrons can be separated into two parts, i.e., $W = W_\perp + W_x$, where $W_x = -\int_0^t e v_x E_x \mathrm{d}t$ refers to the electron energy gained from the longitudinal charge-separation electric field and $W_\perp = -\int_0^t e(v_y E_y + v_z E_z)\mathrm{d}t$ refers to the energy gained from the transverse laser electric field. Figure 3(c) shows that for the high-energy electrons, both the transverse laser field

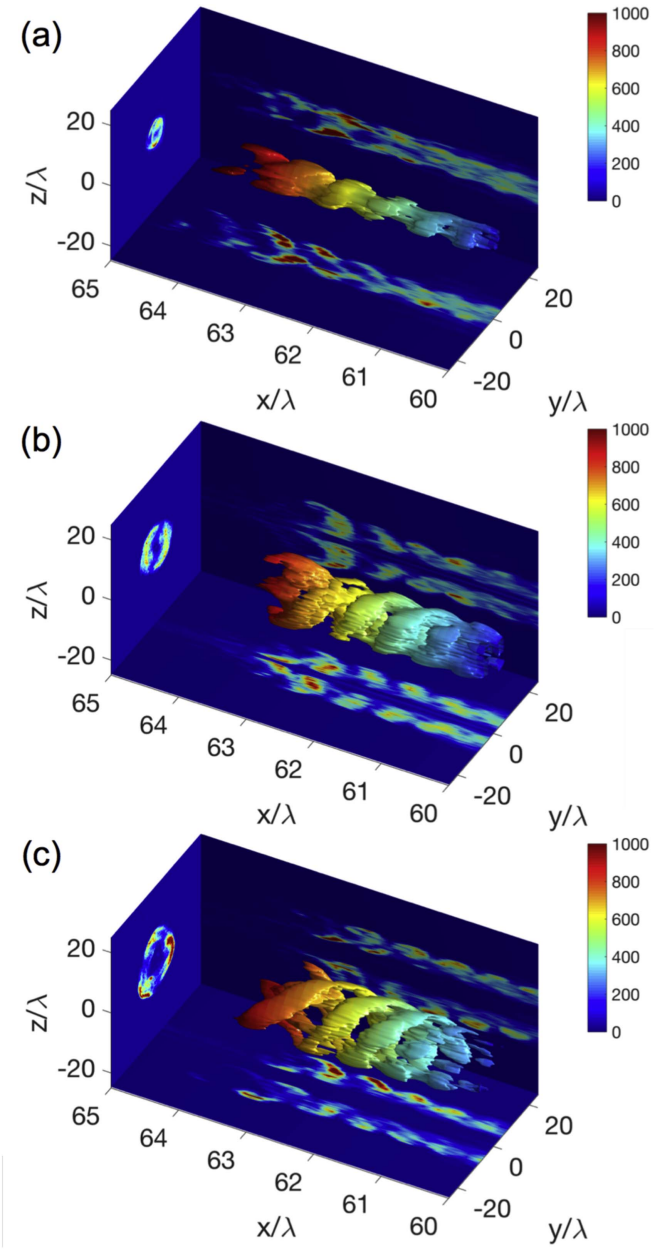

Figure 2. The corresponding 3D energy density distribution of the electron beams with isosurface value of $330 n_c m_e c^2$ for different topological charges, (a) $l = 0$; (b) $l = 1$; (c) $l = 2$.The (y, z) projection plane of the electron energy density on the left is taken at $x = 62.5\lambda$, the (x, y) projection plane at the bottom is taken at $z = 0$, and the (x, z) projection plane at the rear is taken at $y = 0$. The colorbar represents the energy density of the electron beams ranging from 0 to $1000 n_c$ MeV. The number of the sliced electron bunches can be clearly seen in the (y, z) projection plane.

and the longitudinal wake field make great contribution on electron energy gain. In this hybrid regime, both DLA and LWFA play significant roles. In particular, during the interaction with the LG laser field, the electrons gain OAM efficiently from the laser pulse and the topological structure of the accelerated electron beam is manipulated.

3. Theoretical analysis

In this section, we build a theoretical model to explain the emergence of multi-slice helical electron bunches. When the relativistic LG laser pulse propagates into the underdense plasmas, the electrons will be expelled out of the laser region by the laser ponderomotive force to form a stable donut-like plasma bubble, as shown in figure 1(d). Especially when the laser pulse length is comparable with or longer than the plasma bubble length, the electrons in the plasma bubble will interact with both the laser fields and the quasistatic self-generated fields. Taking these fields into consideration in the electron acceleration process, the electron dynamics inside the

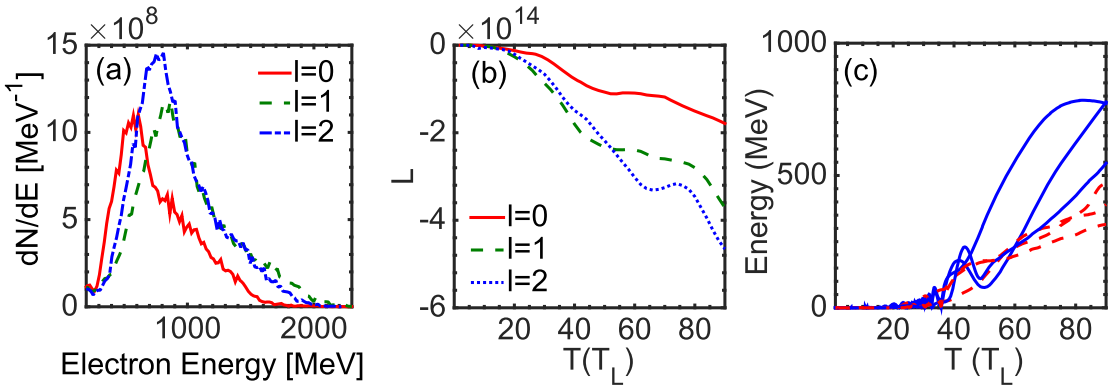

Figure 3. (a) The energy spectra of the helical electron beams for $l = 0$ (red solid line), $l = 1$ (green dashed line), $l = 2$ (blue dotted–dashed line) in the plasma bubble at $100T_L$; (b) the time evolution of the OAM of the electron beams for $l = 0$ (red solid line), $l = 1$ (green dashed line), $l = 2$ (blue dotted–dashed line), where the OAM is in units of $\lambda m_e c = 2.18 \times 10^{-28}$ kg m^2 s^{-1}; (c) the energy gain of three tracing electrons, where $W_x = -\int_0^t ev_x E_x \mathrm{d}t$ (blue solid lines) and $W_\perp = -\int_0^t e(v_y E_y + v_z E_z)\mathrm{d}t$ (red dashed lines).

plasma bubble can be expressed as

$$\frac{\mathrm{d}\vec{p}}{\mathrm{d}t} = -e\left((\vec{E}_L + \vec{E}_S) + \frac{\vec{v}}{c} \times (\vec{B}_L + \vec{B}_S)\right), \tag{2}$$

$$m_e c^2 \frac{\mathrm{d}\gamma}{\mathrm{d}t} = -e\vec{v} \cdot (\vec{E}_L + \vec{E}_S), \tag{3}$$

where $\vec{E}_L$ and $\vec{B}_L$ are the electromagnetic fields of the laser pulse, $\vec{E}_S$ and $\vec{B}_S$ are the quasistatic electric and magnetic fields, respectively. Here a right-hand CP LG laser beam with zero radial index is described as $\vec{E}_L = E_0(\vec{e}_y + \vec{e}_z)\left(\frac{\sqrt{2}r}{r_0}\right)^{|l|} \exp\left(-\frac{r^2}{r_0^2}\right)\exp(\mathrm{i}\phi)$, where E_0 is the amplitude of the laser field, $\phi = \omega_0 t - kx - l\theta$ is the phase of the LG laser pulse, ω_0 is the laser frequency, and k is wavenumber of the laser pulse. The quasistatic fields near the laser propagation axis can be expressed as $\vec{E}_{Sr} = k_E \vec{r}$ and $\vec{B}_{S\theta} = k_B \vec{r}$ [45–47]. Based on these assumptions, the betatron frequency of the electrons that undergo circular motions in the plasma bubble then can be derived as

$$\frac{\mathrm{d}\varphi}{\mathrm{d}t} = \omega_B = \sqrt{\frac{e}{\gamma m_e (v_\parallel k_B + k_E)}}. \tag{4}$$

The laser frequency in the electron co-moving frame can be written as

$$\frac{\mathrm{d}\phi}{\mathrm{d}t} = \omega_\phi = \kappa\omega_0 - l\frac{\mathrm{d}\theta}{\mathrm{d}t} = \omega_L - l\omega_\theta, \tag{5}$$

were $\kappa = 1 - \frac{v_x}{v_{\mathrm{ph}}}$, v_x is the electron velocity along the laser propagation axis, and v_{ph} is the phase velocity of laser in plasma. The first term $\omega_L = \kappa\omega_0$ in equation (5) refers to the Doppler-shifted laser propagation frequency and the second term ω_θ is the angular frequency of laser pulse witnessed by the electron, which is equal to the angular frequency of the circular motion of the electron, i.e., $\omega_\theta = \omega_B$. The electrons can be accelerated by the laser field continuously when the resonance condition $\omega_B \approx \omega_\phi$ is satisfied. To describe the electron motion in the plasma bubble, we further define a relative phase between the electron motion and the laser field as ψ and its time derivative can be written as

$$\frac{\mathrm{d}\psi}{\mathrm{d}t} = \frac{\mathrm{d}\varphi}{\mathrm{d}t} - \frac{\mathrm{d}\phi}{\mathrm{d}t} = \omega_B - \omega_L + l\omega_\theta = (1 + l)\omega_B - \omega_L. \tag{6}$$

The time derivative of electron energy in equation (3) can be rewritten as

$$m_e c^2 \frac{\mathrm{d}\gamma}{\mathrm{d}t} = -ev_\perp E_L \cos\psi - ev_x E_{Sx}. \tag{7}$$

For relativistic betatron electrons with $\gamma \gg 1$, κ, k_B and k_E can be treated as constants as they are slow variables compared to the fast oscillating variables [17, 45–47]. In this case, a Hamiltonian that describes the electron dynamics in phase-space (ψ, γ) can be derived as

$$H = \frac{e}{m_e c^2} v_\perp E_L \sin\psi + \frac{e}{m_e c^2} v_x E_{Sx}\psi + 2(1 + l)\sqrt{\frac{e}{m_e}(v_x k_B + k_E)\gamma} - \omega_L\gamma, \tag{8}$$

where $v_\perp$ is the electron velocity in transverse space and E_L is the amplitude of transverse laser field. In this Hamiltonian system, by letting the right-hand side of equations (6) and (7) become zero, one can get the fixed

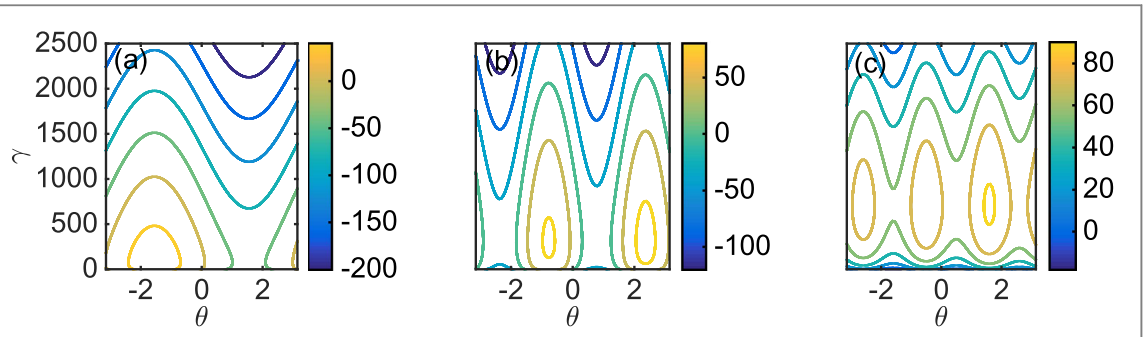

Figure 4. The Hamiltonian and electron trajectories in phase-space (θ, γ) with different topological charges, (a) $l = 0$; (b) $l = 1$; (c) $l = 2$. The normalized parameters $eE_L/m_e\omega_0 c = 70$, $eE_{Sx}/m_e\omega_0 c = 1$, $v_x/c = 0.98$, $v_\perp/c = 0.20$, $k_E = \frac{eE_{Sr}}{m_e\omega_0{}^2} = 5.0$, $k_B = \frac{eB_{S\theta}c}{m_e\omega_0{}^2} = 10.0$, $\phi_L = \pi$ are employed.

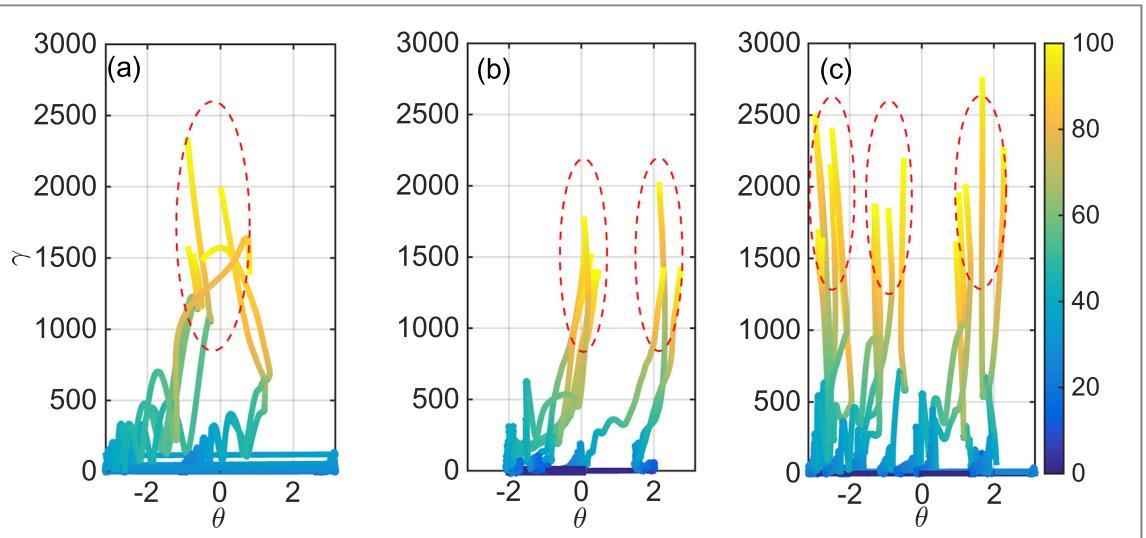

Figure 5. The typical trajectories of the high-energy electrons that are selected from 3D PIC simulations in phase-space (θ, γ) for different topological charges, (a) $l = 0$; (b) $l = 1$; (c) $l = 2$.

points that satisfy the following equations

$$(1 + l)\omega_B - \omega_L = 0, \tag{9}$$

$$-ev_\perp E_L \cos\psi - ev_x E_{Sx} = 0. \tag{10}$$

For equation (10), its solution can be written as $\psi_c = \arccos(-\frac{v_x E_{Sx}}{v_\perp E_L}) + 2n\pi$, where n is integer. Then one can obtain the angular phase of electron motion as

$$\theta_c = \frac{\phi_L + \psi_c}{l + 1}, \tag{11}$$

where $\phi_L = \omega_0 t - kx$ is the laser propagation phase. For simplicity, when the longitudinal charge-separation electric field E_{Sx} is ignored, $\psi_c = \pi/2 + 2n\pi$. Considering that $0 \leqslant \theta_c < 2\pi$, one can get $-\frac{\pi/2+\phi_L}{2\pi} \leqslant n < l + 1 - \frac{\pi/2+\phi_L}{2\pi}$, thus $n = 0, 1, 2\cdots, l$ for a fixed laser propagation phase, e.g., $\phi_L = \pi$. This indicates that the number of fixed points in this Hamiltonian system is $l + 1$, which is determined by the topological charge of the LG laser pulse.

Figure 4 shows the Hamiltonian and trajectories of electrons in phase-space (θ, γ) for a fixed laser propagation phase of $\phi_L = \pi$. It is shown from figure 4(a) that there is only one fixed point and one separatrix for the case of $l = 0$, which is consistent with the previous work [45]. While for the LG laser pulse with $l \neq 0$, the number of fixed points is related to the topological charge of the laser pulse and is equal to $l + 1$, as shown figures 4(b) and (c), which agrees well with the above theoretical estimates. If the electrons are initially located around the fixed points, the acceleration phase of these electrons change slowly so that the electrons can stay in the acceleration phase for a relatively long time and then are efficiently accelerated. However, if the electrons are initially located below the separatrix and away from the fixed points [48], they cannot be accelerated to a high-energy because their orbits are open, as can be clearly seen in figure 4(c). In this case, the electrons would

experience dephasing rapidly and the acceleration process is terminated soon. Thus, the number of fixed points actually determines the acceleration phases for the resonant electrons that can be accelerated to a high-energy. The high-energy electrons would be distributed around the fixed points, and display as multi-slice helical bunches, as demonstrated in figure 2. Figure 5 presents the typical trajectories of high-energy electrons in (θ, γ) phase-space from 3D PIC simulations. It is clearly shown that the high-energy electrons are concentrated around the fixed points described in figure 4. This indicates that the topological charge of the LG laser pulse determines the number of electron bunches that are accelerated in different acceleration phases of the laser electric field. In this way, the topological structure of the accelerated electron beam is controlled by the LG laser pulse.

4. Conclusion

In summary, we propose an approach for producing high-energy helical electron beams based on a hybrid electron acceleration regime by launching an intense LG laser pulse into an underdense plasma. It is shown that due to the special helical phase of the LG laser pulse, when the trapped electrons in the plasma bubble directly interact with the LG laser pulse, the acceleration phase of these electrons is controlled by the topological charge of the LG laser pulse, leading to the generation of multi-slice helical electron bunches. The generated energetic helical electron bunches can be applied to many applications, such as the generation of x/γ-rays with angular momentum [24–28]. The annular beams like these may also be of interest to free-electron-laser applications [23].

Acknowledgments

This work is supported by the National Key R&D Program of China, Grant No. 2016YFA0401100; the National Natural Science Foundation of China (NSFC), Grants No.11575031, No. 11705120, No. 11575298, and No. 91230205, the NSAF U1630246, the China Postdoctoral Science Foundation 2017M612708. The EPOCH code was developed under the UK EPSRC Grants No. EP/G054940/1, No. EP/G055165/1, and No. EP/G056803/1. The authors would like to thank K D Xiao, H X Chang, Q S Feng, C Z Xiao, K Q Pan, Q Wang, Z Xu, W P Yao, W L Zhang, Y X Zhang, X R Xu, H C Zhang, J X Gong and Y X Wang for their useful discussions and helps. L B Ju and T W Huang contribute equally to this work.

ORCID iDs

K Jiang https://orcid.org/0000-0003-0499-4164

References

[1] Allen L, Beijersbergen M W, Spreeuw R J C and Woerdman J P 1992 *Phys. Rev.* A **45** 8185
[2] Beijersbergen M W, Allen L, van der Veen H E L O and Woerdman J P 1993 *Opt. Commun.* **96** 123
[3] Turnbull G A, Robertson D A, Smith G M, Allen L and Padgett M J 1996 *Opt. Commun.* **127** 183
[4] Heckenberg N R, McDuff R, Smith C P, Rubinsztein Dunlop H and Wegener M J 1992 *Opt. Quantum Electron.* **24** S951
[5] Sueda K, Miyaji G, Miyanaga N and Nakatsuka M 2004 *Opt. Express* **12** 3548
[6] Willig K I, Rizzoli S O, Westphal V, Jahn R and Hell S W 2006 *Nature* **440** 935
[7] Padgett M and Bowman R 2011 *Nat. Photon.* **5** 343
[8] Wang J *et al* 2012 *Nat. Photon.* **6** 488
[9] Molina-Terriza G, Torres J P and Torner L 2007 *Nat. Phys.* **3** 305
[10] Tamburini F, Thidé B and Molina G 2011 *Nat. Phys.* **7** 195
[11] Leblanc A, Denoeud A, Chopineau L, Mennerat G, Martin P and Quéré F 2017 *Nat. Phys.* **13** 440
[12] Vieira J, Trines R M G M, Alves E P, Fonseca R A, Mendonça J T, Bingham R, Norreys P A and Silva L O 2016 *Nat. Commun.* **7** 10371
[13] Shi Y, Shen B F, Zhang L G, Zhang X M, Wang W P and Xu Z Z 2014 *Phys. Rev. Lett.* **112** 235001
[14] Vieira J and Mendonça J T 2014 *Phys. Rev. Lett.* **112** 215001
[15] Zhang X M, Shen B F, Shi Y, Wang X F, Zhang L G, Wang W P, Xu J C, Yi L Q and Xu Z Z 2015 *Phys. Rev. Lett.* **114** 173901
[16] Ju L B *et al* 2016 *Phys. Rev.* E **94** 033202
[17] Ju L B, Zhou C T, Huang T W, Jiang K, Zhang H, Wu S Z, Qiao B and Ruan S C 2017 *Phys. Rev.* E **95** 053205
[18] Wang W P, Shen B F, Zhang X M, Zhang L G, Shi Y and Xu Z Z 2015 *Sci. Rep.* **5** 8274
[19] Verbeeck J, Tian H and Schattschneider P 2010 *Nature* **467** 16
[20] Uchida M and Tonomura A 2010 *Nature* **464** 737
[21] McMorran B J, Agrawal A, Anderson I M, Herzing A A, Lezec H J, McClelland J J and Unguris J 2011 *Science* **331** 192
[22] Clark C W, Barankov R, Huber M G, Arif M, Cory D G and Pushin D A 2015 *Nature* **525** 504
[23] Hemsing E, Knyazik A, Dunning M, Xiang D, Marinelli A, Hast C and Rosenzweig J B 2013 *Nat. Phys.* **9** 549
[24] Liu C *et al* 2016 *Phys. Plasmas* **23** 093120

[25] Peele A G, McMahon P J, Paterson D, Tran C Q, Mancuso A P, Nugent K A, Hayes J P, Harvey E, Lai B and McNulty I 2002 *Opt. Lett.* **27** 1752
[26] Sasaki S and McNulty I 2008 *Phys. Rev. Lett.* **100** 124801
[27] Jentschura U D and Serbo V G 2011 *Phys. Rev. Lett.* **106** 013001
[28] Taira Y, Hayakawa T and Katoh M 2017 *Sci. Rep.* **7** 5018
[29] Hemsing E, Dunning M, Hast C, Raubenheimer T and Xiang D 2014 *Phys. Rev. Lett.* **113** 134803
[30] Bahrdt J, Holldack K, Kuske P, Müller R, Scheer M and Schmid P 2013 *Phys. Rev. Lett.* **111** 034801
[31] Tajima T and Dawson J M 1979 *Phys. Rev. Lett.* **43** 267
[32] Pollock B B *et al* 2011 *Phys. Rev. Lett.* **107** 045001
[33] Leemans W P *et al* 2014 *Phys. Rev. Lett.* **113** 245002
[34] Kim H T, Pae K H, Cha H J, Kim I J, Yu T J, Sung J H, Lee S K, Jeong T M and Lee J 2013 *Phys. Rev. Lett.* **111** 165002
[35] Wang X *et al* 2013 *Nat. Commun.* **4** 1988
[36] Faure J, Glinec Y, Pukhov A, Kiselev S, Gordienko S, Lefebvre E, Rousseau J P, Burgy F and Malka V 2004 *Nature* **431** 541
[37] Mangles S P D *et al* 2004 *Nature* **431** 535
[38] Geddes C G R, Toth C, Van Tilborg J, Esarey E, Schroeder C B, Bruhwiler D, Nieter C, Cary J and Leemans W P 2004 *Nature* **431** 538
[39] Liu J S *et al* 2011 *Phys. Rev. Lett.* **107** 035001
[40] Haines M G 2001 *Phys. Rev. Lett.* **87** 135005
[41] Shvets G, Fisch N J and Rax J M 2002 *Phys. Rev.* E **65** 046403
[42] Liseykina T V, Popruzhenko S V and Macchi A 2016 *New J. Phys.* **18** 072001
[43] Arber T D *et al* 2015 *Plasma Phys. Control. Fusion* **57** 113001
[44] Shaw J L, Lemos N, Amorim L D, Vafaei-Najafabadi N, Marsh K A, Tsung F S, Mori W B and Joshi C 2017 *Phys. Rev. Lett.* **118** 064801
[45] Hu R H, Liu B, Lu H Y, Zhou M L, Lin C, Sheng Z M, Chen C E, He X T and Yan X Q 2015 *Sci. Rep.* **5** 15499
[46] Pukhov A, Sheng Z M and Meyer-ter-Vehn J 1999 *Phys. Plasmas* **6** 2847
[47] Huang T W, Robinson A P L, Zhou C T, Qiao B, Liu B, Ruan S C, He X T and Norreys P A 2016 *Phys. Rev.* E **93** 063203
[48] Zhou C T, Zhu S P and He X T 1992 *Phys. Rev.* A **46** 3486